Supercond. Sci. Technol. **21** (2008) 125006 (6pp) doi:10.1088/0953-2048/21/12/125006

A new paradigm for fabricating bulk high-field superconductors

David M J Taylor, Maisoon Al-Jawad and Damian P Hampshire

Superconductivity Group, Physics Department, Durham University, Durham DH1 3LE, UK

E-mail: d.p.hampshire@durham.ac.uk

Received 21 July 2008, in final form 10 September 2008
Published 10 October 2008
Online at stacks.iop.org/SUST/21/125006

Abstract

Superconductivity provides the enabling technology for producing high-field magnets in applications including medical body scanners and particle accelerators. The upper critical field ($B_{C2}(0)$) of the superconductor ultimately limits the field that the magnet can produce. The reports about $PbMo_6S_8$ and Nb_3Sn provide a new method for fabricating high-field superconductors in which superconducting materials are made in nanocrystalline form and the very fine microstructure and high density of defects present are controlled at the nanoscale to significantly increase the electron scattering and hence $B_{C2}(0)$. Here we show direct measurements of $B_{C2}(0)$ for a series of nanocrystalline niobium materials with an unprecedented maximum $B_{C2}(0)$ for bulk Nb of ~3 T. We provide a theoretical description of our results, using the well-established fundamental properties of Nb, that explains why the peak in $B_{C2}(0)$ occurs and can predict optimal $B_{C2}(0)$ for other materials in this new class of nanocrystalline high-field superconductors.

(Some figures in this article are in colour only in the electronic version)

1. Introduction

The use of high magnetic fields for basic physics experiments and medical applications has energized the search for better superconductors with higher current density and magnetic field tolerance over the last 4 decades. For large magnet systems, including the $10 billion superconducting ITER fusion tokamak [1], good strain tolerance is also required. It was shown that one can control the microstructure in nanocrystalline materials to increase the bulk values of the extrapolated upper critical field at zero temperature ($B_{C2}(0)$) in $PbMo_6S_8$ [2, 3] from ~50 to ~100 T. In binary nanocrystalline Nb_3Sn [4], $B_{C2}(0)$ has been increased from ~30 to ~35 T. In this new class of high-field superconductors, which have been fabricated using mechanical milling and hot isostatic pressing, the microstructure and the increased disorder change both the extrinsic properties (e.g. critical current density (J_C)) and the intrinsic properties (e.g. $B_{C2}(0)$). The increases in $B_{C2}(0)$ are understood within the general framework of Ginzburg–Landau–Abrikosov–Gor'kov theory, where a reduced electron mean-free path in the nanocrystalline materials leads to a decrease in the superconducting coherence length and hence an increase in the upper critical field. However to date, the ultimate limit to the increases in $B_{C2}(0)$ and which superconducting materials are likely to produce the best high-field nanocrystalline superconductors has been unknown. In this paper, we present both the normal state and superconducting properties of a series of nanocrystalline niobium samples fabricated using niobium milling media. A record value of $B_{C2}(0)$ for bulk elemental Nb of ~3 T is reported. Because Nb has been extensively studied in the literature and the fundamental properties well-established, and because the upper critical field of all the nanocrystalline material in this work can be directly measured, our general understanding of the interplay between microstructure at the nanoscale and bulk superconductivity is comprehensively investigated. A general theoretical description of the superconducting properties of nanocrystalline superconductors is presented which provides an explanation for the maximum $B_{C2}(0)$ of ~3 T in Nb, at the optimal nanostructure, reported in this paper.

2. Experimental details

Niobium powder (99.98%) was mechanically milled for different time periods up to 230 h using a Fritsch P6 planetary ball miller operating at a rotational velocity of

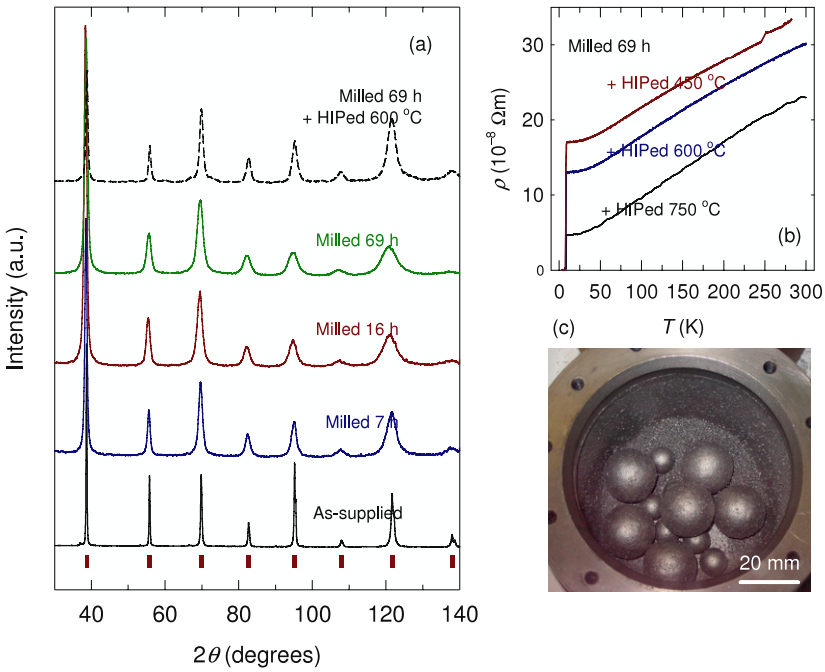

Figure 1. X-ray diffraction spectra and resistivity of conventional and nanocrystalline niobium. (a) X-ray diffraction spectra of unmilled, milled, and milled-and-HIPed niobium. (b) Resistivity as a function of temperature for niobium milled for 69 h and hot isostatically pressed at 750 (#2), 600 (#3) and 450 °C (#4). (c) Photo of the milling vessel after 3 h milling.

Table 1. Properties of conventional (#1) and nanocrystalline niobium (#2–5). T_C: critical temperature. $B_{C2}(0)$: upper critical field. γ: Sommerfeld constant. $\bar{\omega}_1$, $\bar{\omega}_{log}$: electron–phonon moments. $\theta_D(0)$: Debye temperature. ρ_n: resistivity. l: electron mean-free path and λ: electron–phonon coupling parameter.

Sample	#1	#2	#3	#4	#5
Milling time (h)	0	69	69	69	69
HIP temp. (°C)	—	750	600	450	—
Grain size (nm)	∼100	15	8	6	6
T_C (K)	9.14	8.27	7.58	7.11	5.53
$(\partial B_{C2}/\partial T)_{T_C}$ (T K^{-1})	0.08	0.36	0.46	0.53	0.71
$B_{C2}(0)$ (T)	0.57	2.28	2.76	3.00	3.17
γ (J K^{-2} m^{-3})	680	630	585	590 ± 25	525
$\theta_D(0)$ (K)	242	252	242	237	270
$\bar{\omega}_1$, $\bar{\omega}_{log}$ (K)	161, 131	167, 136	166, 134	165, 132	175, 145
ρ_n meas. (calc.) ($\mu\Omega$ cm)	(0.8)	5 (9.9)	13 (14)	17 (17)	(26)
l (nm)	51	4.1	2.8	2.5	1.6
λ	0.93	0.87	0.83	0.81	0.71

300 revolutions min^{-1}. The milling was performed under argon gas with a niobium milling pot and niobium balls (6 × 20 mm and 6 × 10 mm diameter), and with an initial ball-to-powder weight ratio of ∼14:1. Ball milling was performed in 30 min cycles for the first 10 h of milling. After each 30 min cycle, the milling pot was opened under argon gas and the niobium was recovered from the pot walls and the surfaces of the balls. This recovery process was necessary in the early stages in order to provide sufficient powder yield in the later stages. The powder milled for 69 h was subsequently hot isostatically pressed (HIPed) at a pressure of 2000 bar and at temperatures of 450, 600 and 750 °C for up to 5 h. AC susceptibility and x-ray diffraction (XRD) measurements were performed on all samples, while additional specific heat measurements were performed on the five samples presented here and labelled #1–5: the as-supplied unmilled powder (#1), the samples milled for 69 h and HIPed at 750 (#2), 600 (#3) and 450 °C (#4), and the powder milled for 69 h (#5). The increasing label numbers indicate increasing levels of disorder at the nanoscale (see table 1). Resistivity measurements were also performed on the bulk HIPed samples. The XRD measurements were carried out using a Bruker D8 powder diffractometer, and the other measurements using a Quantum Design PPMS system.

Figure 1(a) shows XRD spectra for unmilled (as-supplied), milled, and milled-and-HIPed niobium. The peaks broaden with increasing milling time. Approximate grain sizes were calculated via Rietveld refinement (using the TOPAS software package) and ignoring any broadening due to micro-strain. The niobium milled for 69 h has an average grain size of 6 nm and was chosen for HIPing since further decreases in grain size were not observed after longer

milling times up to 230 h [6]. Previous limited bright-field TEM on milled $PbMo_6S_8$ samples confirmed that XRD gives a reasonable indication of the grain size [5] but detailed microscopy is required to characterize the different types of disorder and measure the distribution and size of the grains accurately. Approximate grain sizes for samples #1–5 are shown in table 1. The peaks in the XRD spectra narrow with increasing HIP temperature, indicating increasing grain growth. Figure 1(b) shows the temperature dependence of the normal-state resistivity for the milled and HIPed samples. The low-temperature normal-state resistivity ($\rho(10\ \mathrm{K})$) decreases with increasing HIP temperature consistent with increasing grain size and increasing structural order. Also shown, in figure 1(c), is a photograph of the milling pot after milling for 3 h. Note that the niobium powder forms approximately spherical agglomerates with a typical diameter of 0.25 mm.

The superconducting properties were measured using specific heat capacity (c_P) and AC magnetic susceptibility (χ'). Figure 2 shows the experimental data for the sample milled for 69 h and HIPed at 450 °C. The inset to figure 2(a) shows the specific heat data for the unmilled material, and demonstrates the considerable differences in the field tolerance between the conventional and nanocrystalline materials. The characteristic temperature for the superconducting transition is obtained from the heat capacity data by constructing an idealized, infinitely sharp transition that conserves entropy. The magnitude of the heat capacity jump for the nanocrystalline material and the conventional material are similar, demonstrating that the upper critical field values in this work ($B_{C2}^{c_P}(T)$) are characteristic of bulk material. For the AC susceptibility data, $B_{C2}^{\chi'}(T)$ is defined where the real part of the susceptibility equals -0.1, which gives good agreement with the specific heat results (see the inset to figure 3(a)).

The $B_{C2}(T)$ results for the powders milled for different time periods are shown in figure 3(a). Figure 3(b) shows the $B_{C2}(T)$ results for samples #1–5. In order to extrapolate to $T = 0$, the data are fitted by the function $B_{C2}(t) \propto (1 - t^2)(1.6 - 0.6t)$ with $t = T/T_C$, where the first term approximates the temperature dependence of the thermodynamic critical field [7] and the second term approximates the temperature dependence of the Ginzburg–Landau parameter [8]. The inset to figure 3(b) shows that this function is valid for all of the samples #1–5.

When producing high quality nanocrystalline materials, the issues of contamination and oxidization are critical because of the large surface area to volume ratio. Standard chemical safety sheets warn that even 5 micron Nb powder can autoignite at room temperature [9]. We have taken particular care to retain pure elemental niobium in this work by using niobium milling media and completing all processing under high purity argon (to avoid contamination and oxidization respectively). The values of T_C and $B_{C2}(0)$ for samples #1–5 are summarized in table 1. Work in the literature on the effects of interstitial oxygen on the superconductivity of niobium shows that if the reduction in T_C of sample #2 compared to the as-supplied material were entirely due to oxygen, the contamination would be less than 0.5 at.% oxygen and the contribution to $B_{C2}(0)$ would be about 1 T [10].

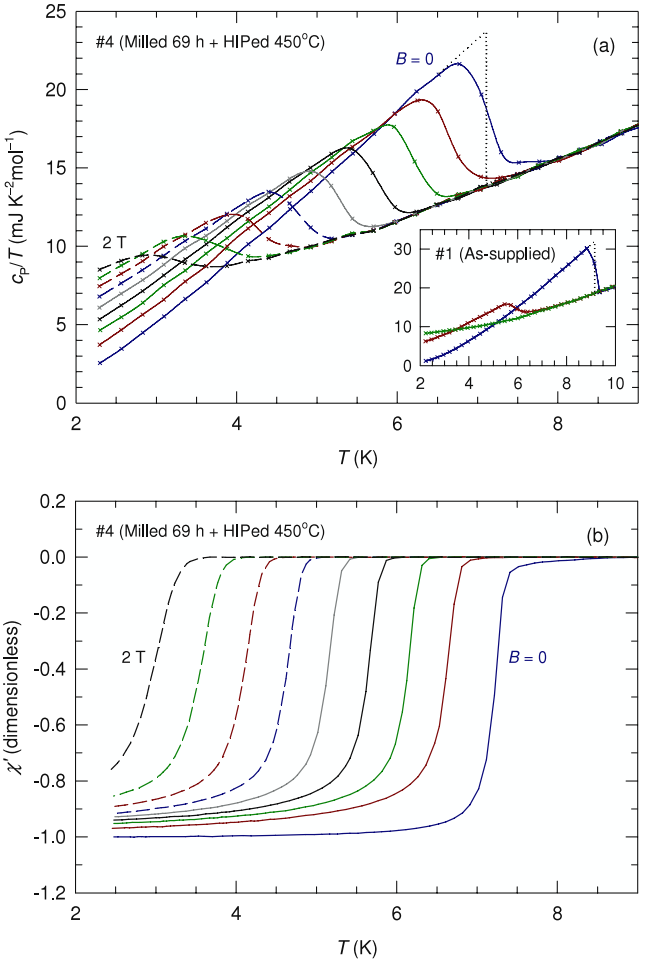

Figure 2. Specific heat and magnetic susceptibility data for nanocrystalline niobium (sample #4). (a) Specific heat data (symbols) as a function of temperature at 0.25 T magnetic field increments. The dotted lines show an example of the constructed idealized transition. The inset shows equivalent heat capacity data for the as-supplied material (#1). (b) Real part of the AC susceptibility as a function of temperature at 0.25 T magnetic field increments.

The recovery of T_C towards the original value with increased HIPing temperature shown by samples #4 to #2 in table 1 suggests that HIPing at higher temperature would lead T_C to further recover towards the original as-supplied T_C value. We conclude that the levels of contamination in the Nb samples reported here are very low indeed and are not responsible for the properties reported.

3. Analysis

Table 1 shows the Sommerfeld constant γ, the Debye temperature $\theta_D(T = 0)$ and the moments $\bar{\omega}_1$ and $\bar{\omega}_{\log}$ of the electron–phonon spectrum function $\alpha^2F(\omega)$ [11]. These parameters were calculated by fitting the normal-state specific heat data, obtained from high-field measurements above B_{C2} [11, 12]. The moments are calculated by assuming that the electron–phonon coupling characteristic $\alpha^2 \propto \omega^{-0.5}$ (ω is the frequency), which gives good agreement with the results of tunnelling measurements [11, 13]. It can be seen

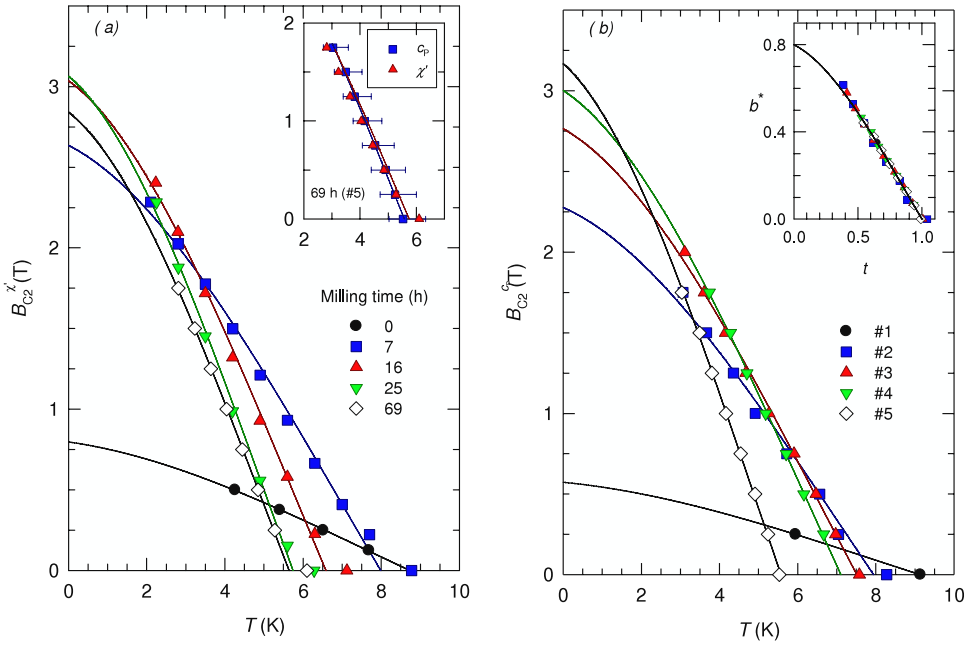

Figure 3. The upper critical field as a function of temperature for conventional and nanocrystalline niobium. (a) AC susceptibility results for powders milled for different time periods. Inset: comparison of AC susceptibility and specific heat results for the 69 h milled powder. (b) Specific heat results for bulk samples #1–5. Inset: reduced upper critical field ($b^* = B_{C2}/[T_C(\mathrm{d}B_{C2}/\mathrm{d}T)_{T_C}]$) versus reduced temperature (t) for samples #1–5.

from the experimental data in figure 3 and table 1 that there is a monotonic decrease in the critical temperature and the Sommerfeld constant and a monotonic increase in the gradient $[(\mathrm{d}B_{C2}/\mathrm{d}T)_{T_C}]$ as the disorder at the nanoscale increases.

The upper critical field at zero temperature can be related to various microscopic properties of the material via the following GLAG theory expression [7, 14]:

$$B_{C2}(0) = 0.973\mu_0^{1/2}\eta\kappa^*(0,\lambda_{tr})\,R\,(\lambda_{tr})^{-1} \times \left[7.30\times10^{37}\,(\gamma T_C/S)^2 + 2.78\times10^6\gamma T_C\rho_n\right] \quad (1)$$

where $\eta \approx 1$ is a strong-coupling correction [7], $\kappa^*(0,\lambda_{tr})$ is the ratio of the Ginzburg–Landau parameter at zero temperature to that at the critical temperature, which was shown above to be approximately equal to 1.6 for all of the samples, $R(\lambda_{tr}) \approx 1$ is part of the Gor'kov function [14], $\lambda_{tr} = 3.81\times10^{-32}S^2\rho_n/(\gamma T_C)$ is the impurity parameter [14], and S is the Fermi surface area. The anisotropy of the Fermi surface [8], additional strong-coupling theory modifications [15], and Pauli paramagnetic limiting [16] all have relatively small effects on the results of equation (1) [7].

The critical temperature of disordered superconductors can be expressed as [17–20]:

$$k_B T_C = \frac{\hbar\bar{\omega}_1}{1.20}\exp\left(-\frac{1.04\,(1+\lambda)}{\lambda-\mu^*\,[1+0.62\lambda]}\right), \quad (2)$$

where λ is the electron–phonon coupling parameter and μ^* is the Coulomb pseudopotential [20]. The electron–phonon coupling parameter can be approximated by $\lambda \propto N(E_F)$ where $N(E_F)$ is the unrenormalized electronic density of states at the Fermi surface [17]. $N(E_F)$ can be related to the experimental values of the Sommerfeld constant derived from heat capacity data via $\gamma = \frac{2}{3}\pi^2 k_B^2 N(E_F)(1+\lambda)$.

In order to describe the decrease in γ with increasing resistivity, we use a simplified version of the lifetime broadening model. The peak in the density of states at the Fermi energy is modelled by a Lorentzian of half-width E_0, where the broadening function is a Lorentzian with half-width $\hbar/\tau$ and $\tau = 1.65\times10^{19}\gamma/(S^2\rho_n)$ is the mean scattering time. This leads to [21, 22]:

$$N(E_F) = N_0(E_F)\left(\frac{(4/\pi)\,(\hbar/\tau E_0)\tan^{-1}(\hbar/\tau E_0) - 1}{(\hbar/\tau E_0)^2 - 1}\right). \quad (3)$$

Figure 4 shows the variation of $B_{C2}(0)$ with T_C calculated for increasing resistivity in Nb and Nb_3Sn. The calculation was carried out using the free parameters shown in table 2 and assuming constant phonon frequencies. For superconductors with strong-coupling constants, increased scattering decreases T_C [20] and γ whereas $B_{C2}(0)$ and ρ increase. Eventually $B_{C2}(0)$ reaches its peak value as decreases in T_C and γ compensate for increases in ρ. The maximum value of $B_{C2}(0) \approx 3$ T for nanocrystalline niobium is similar to the calculated limit (~3.5 T) for the upper critical field in niobium. We note that isolated nanocrystalline grains of Nb embedded in an amorphous Nb–O matrix have been reported in thin films with $B_{C2}(0)$ of ~6.6 T, which is consistent with a surface barrier in these grains of 1.69 times the optimized bulk value we have found of ~3.5 T, and a size-induced Kubo gap [23, 24]. Also shown in figure 4 is a comparison with experimental data from Orlando for Nb_3Sn [14, 25]. Again theory predicts a peak in $B_{C2}(0)$ of ~35 T consistent with optimized nanocrystalline and doped results [4, 14, 25].

Detailed considerations of microscopic theory suggest that disorder not only affects T_C through the density of states but

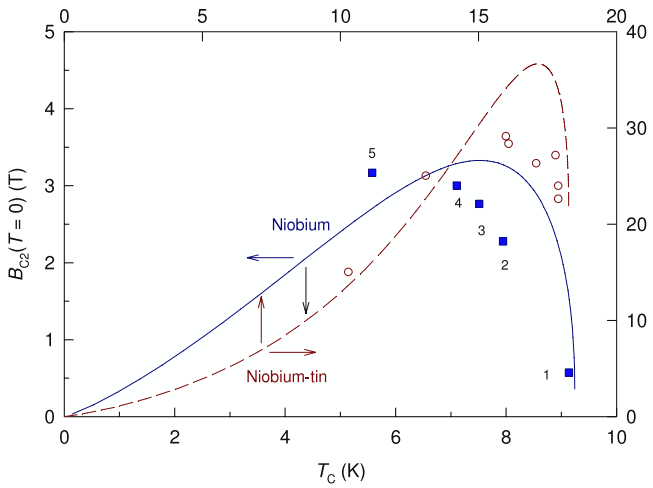

Figure 4. Theoretical upper critical field of nanocrystalline niobium and niobium–tin. Upper critical field as a function of critical temperature for niobium and niobium–tin with different levels of disorder. The lines show the theoretical values obtained by increasing the resistivity. The symbols show the experimental data (data for the niobium samples are labelled #1–5). The data for Nb_3Sn were taken from Orlando [14, 25].

Table 2. Free parameters used to calculate the resistivity dependence of the upper critical field and the critical temperature. κ^*: the ratio of the Ginzburg–Landau parameter at zero temperature to that at the critical temperature. γ: Sommerfeld constant. S: Fermi surface area. $\bar{\omega}_1$, $\bar{\omega}_{\log}$: electron–phonon moments. λ: electron–phonon coupling parameter. μ^*: Coulomb pseudopotential and E_0: half-width in the peak of the density of states.

Parameter	Nb	Nb_3Sn
κ^*	1.6	1.20–1.26
γ (J K^{-2} m^{-3})	680	1176
S (10^{21} m^{-2})	3.74	1.5
$\bar{\omega}_1$, $\bar{\omega}_{\log}$ (K)	162, 150	152, 125
λ	0.93	1.8
μ^*	0.116	0.14
E_0 (meV)	250	60

also through the electron–phonon, Coulomb and self-energy interactions [20]. The strength of these additional effects is not yet well-known. If we simply add these effects with a strength proposed for simple metals and A15 compounds [20] to the effects of lifetime broadening, the peak value of $B_{C2}(0)$ reduces by an additional ∼0.5 and ∼5 T for Nb and Nb_3Sn respectively [20]. The results in figure 4 confirm that the additional reduction in the maximum $B_{C2}(0)$ from these additional microscopic effects cannot be large.

4. Discussion and concluding comments

The local electronic properties of these nanocrystalline materials within the grains and across the grain boundaries is an important area for future investigation. The values of $B_{C2}(0)$ measured imply an electron mean-free path of ∼1 nm in the Nb nanocrystalline materials with a grain size ∼10 nm. Hence, as with nanocrystalline $PbMo_6S_8$, the grain boundaries alone are not sufficiently dense to explain the high $B_{C2}(0)$ values obtained [2]. Rather, the interior of the grains themselves must be highly disordered. In this context, the milling decreases the grain size and increases the scattering within the grains, and the HIP treatment reverses these processes in a controlled way that allows us to identify the disorder/microstructure that optimizes $B_{C2}(0)$. Nanocrystalline materials which exhibit technologically-important properties such as increased mechanical strength [26], increased chemical reactivity and improved magnetic properties [27], can have added to this list improved upper critical field.

Powder-in-tube technology is well-established for fabricating long wires and tapes for industrial applications in both LTS and HTS materials [28]. In the traditional optimization process, the intrinsic properties (e.g. $B_{C2}(0)$ and T_C) are kept as high as possible while pinning sites (e.g. grain boundaries) are introduced to increase extrinsic properties (e.g. J_C). In this new paradigm for making high-field superconductors and magnets, highly disordered or amorphous powder (for example produced using milling) can be inserted into tubes and drawn to produce conductors that can then be wound into coils. The coils can then be HIPed (i.e. heat treated under pressure) using conditions chosen to optimize J_C at the operating field and temperature of the magnet by controlling pinning, $B_{C2}(0)$ and T_C. Although one can expect the disordered materials to have degraded T_C, there can be a very marked increase in the upper critical field at the operating temperature of the magnet (typically ∼2–5 K for low-temperature superconductors). In these new high-field magnets, the distinction between intrinsic and extrinsic superconducting properties becomes blurred as microstructure and intragranular scattering on the nanoscale control both.

References

[1] Aymar R 2001 ITER R&D: executive summary: design overview *Fusion Eng. Des.* **55** 107–18
[2] Niu H J and Hampshire D P 2003 Disordered nanocrystalline superconducting $PbMo_6S_8$ with very large upper critical field *Phys. Rev. Lett.* **91** 027002
[3] Hampshire D P and Niu H J 2003 *International Patent Number* WO03/094251 A22002
[4] Cooley L D, Hu Y F and Moodenbaugh A R 2006 Enhancement of the upper critical field of Nb_3Sn utilizing disorder introduced by ball milling the elements *Appl. Phys. Lett.* **88** 142506
[5] Niu H J and Hampshire D P 2002 Fabrication of nanocrystalline and amorphous Chevrel phase $PbMo_6S_8$ powder by ball milling *Physica* C **372** 1145–7
[6] Koch C C 1997 Synthesis of nanostructured materials by mechanical milling: problems and opportunities *Nanostruct. Mater.* **9** 13–22
[7] Carbotte J P 1990 Properties of Boson-exchange superconductors *Rev. Mod. Phys.* **62** 1027–157
[8] Weber H W *et al* 1991 Anisotropy effects in superconducting niobium *Phys. Rev.* B **44** 7585–600
[9] http://www.espi-metals.com/msds's/niobium.htm2008
[10] Koch C C, Scarbrough J O and Kroeger D M 1974 Effects of interstitial oxygen on the superconductivity of niobium *Phys. Rev.* B **9** 888–97
[11] Junod A, Jarlborg T and Muller J 1983 Heat capacity analysis of a large number of A15-type compounds *Phys. Rev.* B **27** 1568–85

[12] Junod A 1980 Calcul des frequences moyennes de phonons utiles en supraconductivite a partir de la chaleur specifique *Solid State Commun.* **33** 55–8
[13] Wolf E L, Zasadzinski J, Osmun J W and Arnold G B 1980 Proximity electron-tunnelling spectroscopy 1: experiments on Nb *J. Low Temp. Phys.* **40** 19–50
[14] Orlando T P, McNiff E J, Foner S and Beasley M R 1979 Critical fields, Pauli paramagnetic limiting, and material parameters of Nb_3Sn and V_3Si *Phys. Rev.* B **19** 4545–61 LP–61
[15] Schossmann M and Schachinger E 1986 Strong-coupling theory of the upper critical magnetic field H_{c2} *Phys. Rev.* B **33** 6123–31
[16] Werthamer N R, Helfand E and Hohenberg P C 1966 Temperature and purity dependence of the superconducting critical field, H_{C2}. III. Electron spin and spin–orbit effects *Phys. Rev.* **147** 295–302
[17] McMillan W L 1968 Transition temperature of strong coupled superconductors *Phys. Rev.* **167** 331–44
[18] Allen P B and Dynes R C 1975 Transition temperature of strong-coupled superconductors reanalyzed *Phys. Rev.* B **12** 905–22
[19] Belitz D 1987 Theory for dirty superconductors. II. McMillan solution and T_C degradation *Phys. Rev.* B **35** 1651–8
[20] Belitz D 1987 Theory of disorder-induced increase and degradation of superconducting T_C *Phys. Rev.* B **36** 47–53
[21] Camerlingo C, Scardi P, Tosello C and Vaglio R 1985 Disorder effects in ion-implanted niobium thin films *Phys. Rev.* B **31** 3121–3
[22] Testardi L R and Mattheiss L F 1978 Electron lifetime effects on properties of A15 and BCC materials *Phys. Rev. Lett.* **41** 1612–5
[23] Bose S, Raychaudhuri P, Banerjee R, Vasa P and Ayyub P 2005 Mechanism of the size dependence of the superconducting transition of nanostructured Nb *Phys. Rev. Lett.* **95** 224502
[24] Bose S, Raychaudhuri P, Banerjee R and Ayyub P 2006 Upper critical field in nanostructured Nb: competing effects of the reduction in density of states and the mean free path *Phys. Rev.* B **74** 147003
[25] Orlando T *et al* 1981 The role of disorder in maximizing the upper critical field in the Nb–Sn system *IEEE Trans. Magn.* **17** 368–9
[26] Valiev R 2004 Nanostructuring of metals by severe plastic deformation for advanced properties *Nat. Mater.* **3** 511–6
[27] Gleiter H 1989 Nanocrystalline materials *Prog. Mater. Sci.* **33** 223–315
[28] Larbalestier D C, Gurevich A, Feldmann D M and Polyanskii A 2001 High-T_C superconducting materials for electric power applications *Nature* **414** 368–77